Chen et al. *Zool. Res.* 2025, 46(6): 1516−1530
https://doi.org/10.24272/j.issn.2095-8137.2025.155
https://cstr.cn/32248.14.zr.2025.155

ZR | Zoological Research

Article Open Access

Single-cell transcriptomics reveals dynamic reprogramming of testicular immunity in *Brucella*-infected goat testis

Wen-Bo Chen[1], Cong-Liang Wang[1], Shi-Cheng Wan[1], Xuan Luo[1], Dong-Hui Yang[1,5], Meng-Fei Zhang[1,6], Wen-Ping Wu[1], Na Li[1], Bin Han[4], Hai-Jing Zhu[3,*], Hai-Sheng Yu[2,*], Jin-Lian Hua[1,*]

[1] *College of Veterinary Medicine*, *Shaanxi Centre of Stem Cells Engineering & Technology*, *Northwest A & F University*, *Yangling*, *Shaanxi* 712100, *China*

[2] *Guangzhou Eighth People's Hospital*, *Guangzhou Medical University*, *Guangzhou*, *Guangdong* 510440, *China*

[3] *Shaanxi Provincial Engineering and Technology Research Center of Cashmere Goats*, *Life Science Research Center*, *Yulin University*, *Yulin*, *Shaanxi* 719000, *China*

[4] *Yulin Animal Husbandry and Veterinary Service Center*, *Yulin*, *Shaanxi* 719000, *China*

[5] *Laboratory of Animal Disease Model*, *College of Veterinary Medicine*, *Sichuan Agricultural University*, *Chengdu*, *Sichuan* 611130, *China*

[6] *College of Veterinary Medicine*, *Xinjiang Agricultural University*, *Urumqi*, *Xinjiang* 830000, *China*

ABSTRACT

Brucellosis, a zoonotic disease caused by *Brucella* infection, poses a major threat to both global health and livestock productivity. Although reproductive impairment is well established, the molecular mechanisms driving testicular immunopathology remain poorly understood. In this study, single-cell RNA sequencing was used to delineate transcriptional changes in goat testicular tissues under physiological and *Brucella*-infected conditions, revealing dynamic immunological remodeling of the testicular microenvironment. Infection induced marked shifts in T cell and macrophage phenotypes, with T cells exhibiting pronounced hyperactivation linked to CD45-mediated signaling cascades. Thioredoxin-interacting protein (*TXNIP*), a gene strongly up-regulated in response to infection, emerged as a potential immunotherapeutic target. Intercellular communication networks were significantly disrupted in infected testes, with CD39- and JAM-dependent signaling pathways implicated in the erosion of immune privilege. Regulon analysis further identified GATA3, IRF5, SEMA4A, and HCLS1 as transcriptional regulators associated with T cells and macrophages in infected testes. These findings provide novel insights into the molecular mechanisms driving testicular immunopathology during *Brucella* infection and highlight candidate targets for immunomodulatory intervention in disease control and livestock reproductive health.

Keywords: *Brucella* infection; Brucellosis; Single-cell RNA sequencing (scRNA-seq); Immune response; *TXNIP*

INTRODUCTION

Brucellosis, caused by members of the *Brucella*e genus, represents a pervasive zoonotic infection that severely impacts both livestock productivity and human health (Byndloss & Tsolis, 2016; Dorneles et al., 2015; Liu et al., 2024c; Qureshi et al., 2023; Yu et al., 2022). These pathogens display pronounced tropism for reproductive tissues, leading to a spectrum of reproductive pathologies, including spontaneous abortion, orchitis, epididymitis, and infertility, which collectively result in substantial global economic losses (Byndloss & Tsolis, 2016; Savasci et al., 2014; Yu et al., 2022). Goats (*Capra hircus*), widely utilized for dairy, meat, and fiber production, serve as principal reservoirs for *Brucella melitensis*, a highly virulent zoonotic pathogen in humans (Byndloss & Tsolis, 2016; Pappas et al., 2005; Yu et al., 2022). Although electron microscopy has illuminated key aspects of *Brucella* behavior *in vitro* (Celli et al., 2003; Sedzicki et al., 2018), the mechanisms by which the pathogen perturbs germline architecture and somatic testicular compartments, such as Sertoli and Leydig cells, remain poorly characterized.

Received: 22 June 2025; Accepted: 10 September 2025; Online: 11 September 2025

Foundation items: This work was supported by the National Key Research and Development Program of China (2023YFF1000904, 2022YFD1302201), National Natural Science Foundation of China (32372970，U24A20438), Key Technologies Demonstration of Animal Husbandry in Shaanxi Province (2025NYGG005, 2024NYGG005), Inner Mongolia Autonomous Region Open Competition Projects (2022JBGS0025), and Open Fund Project of the National Key Laboratory of Veterinary Public Health and Safety (2025SKLVPHS08)

*Corresponding authors, E-mail: haijingzhu@yulinu.edu.cn; yuhaisheng@gzhmu.edu.cn; jinlianhua@nwsuaf.edu.cn

Spermatogenesis is a tightly orchestrated, multi-stage developmental program critical for male fertility, encompassing mitotic proliferation of spermatogonial stem cells (SSCs), meiotic division of spermatocytes, and terminal differentiation of haploid spermatids (Chen et al., 2024a; Rabbani et al., 2022). These processes are governed by stage-specific transcriptional programming and rely on functional coordination with the somatic niche. The testicular microenvironment is composed of diverse somatic cell types, including Sertoli cells, Leydig cells, peritubular myoid cells, and resident macrophages (Chen et al., 2024a), all of which establish physical and paracrine signaling networks with developing germ cells (Oatley & Brinster, 2012). Crucially, dynamic crosstalk among somatic compartments, mediated by cytokines and tight junctions, is essential for maintaining metabolic support, immune tolerance, and differentiation fidelity throughout spermatogenesis (Guo et al., 2021; Oatley & Brinster, 2012).

Brucella, a facultative intracellular pathogen, has evolved a type IV secretion system (T4SS) to establish replicative niches in endoplasmic reticulum-derived vacuoles within host phagocytes such as macrophages and dendritic cells (Byndloss & Tsolis, 2016; Celli, 2019; De Bolle et al., 2015; Fugier et al., 2007). This intracellular strategy facilitates immune evasion and persistence within the testicular microenvironment (Byndloss & Tsolis, 2016; Celli, 2019; Celli et al., 2003). *Brucella* infection also induces aberrant inflammasome activation in macrophages, disrupts Sertoli-germ cell adhesion via metalloprotease secretion, and initiates proinflammatory signaling that depletes SSC populations, thereby impairing spermatogenesis and promoting subfertility (Byndloss & Tsolis, 2016; Miraglia et al., 2013; Yu et al., 2022). Elucidating the molecular disruptions underlying these pathologies is critical for advancing brucellosis control strategies.

Recent advances in single-cell transcriptomics have revolutionized the deconvolution of complex biological systems, providing a transformative platform for dissecting tissue heterogeneity and cellular dynamics at high resolution (Hao et al., 2024; Stuart et al., 2019). Previous studies have applied single-cell RNA sequencing (scRNA-seq) to investigate testicular development and pathology (Alfano et al., 2021; Di Persio et al., 2021; Guo et al., 2021; Sohni et al., 2019). In the present study, scRNA-seq was performed on testicular tissue from a *Brucella*-infected 6-year-old goat and compared with healthy goat data (Yu et al., 2021), generating a dataset comprising 15 179 single-cell transcriptomes. Infection induced widespread transcriptional remodeling across testicular somatic cells. Notably, thioredoxin-interacting protein (*TXNIP*) emerged as a key differentially expressed gene (DEG) and hub of immune cell-enriched co-expression modules identified though weighted gene co-expression network analysis (WGCNA), suggesting a central role in anti-*Brucella* responses. Immunohistochemical staining confirmed elevated TXNIP expression in infected testicular tissue. To further resolve immune dynamics, pseudotime trajectory analysis of T cells, construction of cell-cell communication networks, and gene regulatory networks were performed. Collectively, these analyses uncovered substantial remodeling of adaptive immune responses, including altered intercellular communication networks and transcriptional regulation. Notably, the study identified key immune-associated regulons and signaling pathways that may contribute to the breakdown of testicular immune privilege. Collectively, these findings provide mechanistic insights into Brucella-induced testicular immunopathology and identify candidate molecular targets for therapeutic intervention and reproductive health management in livestock.

MATERIALS AND METHODS

Brucella-infected goat testicular sample collection and dissociation

All procedures involving brucellosis-infected testicular samples were approved by the Bioethics and Biosafety Prevention and Control Management Committee of Yulin University (Approval No. 2022051306). Testes were collected from a brucellosis-infected 6-year-old goat at the Yulin Animal Husbandry and Veterinary Service Center and processed under biosafety level 3 (BSL-3) containment at Guangzhou Eighth People's Hospital, China.

Testicular tissue was processed within 24 h post-collection. Samples were washed three times with pre-cooled Dulbecco's phosphate-buffered saline (DPBS), mechanically disrupted, and sectioned into small fragments. The tissue fragments were incubated in dissociation buffer containing 2 mg/mL collagenase IV and 0.25 mg/mL DNase I in 0.25% trypsin-EDTA at 37°C for 15 min. Every 5 min, tissues were gently triturated using a P1000 pipette against the bottom of an Eppendorf tube; this process was repeated three times. Digestion was terminated by adding an equal volume of Dulbecco's modification of Eagle's medium (DMEM) containing 10% fetal bovine serum (FBS). Single-cell suspensions were prepared from enzymatically dissociated testicular parenchyma, excluding connective tissue capsules. Cell suspensions were sequentially passed through 100 μm and 40 μm strainers, then centrifuged at 4°C and 1 000 ×*g* for 5 min, and washed with precooled DPBS. The resulting cell pellet was resuspended in PBS containing 0.4% bovine serum albumin (BSA) at a final concentration of approximately 1 000 cells/μL for scRNA-seq.

ScRNA-seq library preparation and sequencing

A target capture of approximately 8 000–9 000 cells was achieved using the 10x Chromium X platform. Cells were diluted according to the manufacturer's instructions, and library preparation was conducted using a Chromium Next GEM Single Cell 3' Reagent Kit v.3.1. High-throughput library sequencing was performed using the Illumina sequencing platform (NovaSeq 6000, USA) at LC-Bio Technology (China).

Processing of scRNA-seq data

Raw data were demultiplexed using the "mkfastq" function in Cell Ranger v.6.1.2 to generate FASTQ files. Reads were aligned to the ARS1.2 goat reference genome using STAR, followed by filtering and UMI counting via the "count" function with default settings. Only reads confidently mapped to exonic regions with at least 65% alignment were retained. Valid barcodes accounted for 98.2% of the dataset. A total of 8 479 high-quality single-cell transcriptomes were retained for downstream analysis.

Rose-Bengal plate agglutination test

The Rose-Bengal plate agglutination test was used for serological confirmation of *Brucella* infection in precipitated serum. Blood (2 mL) was collected from the jugular vein using a disposable needle and sterile collection tube. Serum was allowed to precipitate for 2 h before serological testing. For the

test, 20 μL of serum was mixed with Rose Bengal antigen (tiger red) on a test plate via gentle pipetting and incubated at room temperature (RT) for 5 min. Standard positive and negative serum samples were used as controls. Positive reactions were identified by the appearance of flocculent or sand-like agglutination, while negative samples remained unchanged. All positive samples were retested for confirmation. Reproducible agglutination was considered indicative of *Brucella* infection.

Hematoxylin and eosin staining

Testicular tissue (~1–3 cm^2) from *Brucella*-infected goat was fixed in 4% paraformaldehyde for 48 h and subsequently embedded in paraffin. Sections from both infected samples and archival paraffin blocks of normal testis (Yu et al., 2021) were deparaffinized through sequential immersion in dimethylbenzene I (8 min), dimethylbenzene II (8 min), anhydrous ethanol I (6 min), anhydrous ethanol II (6 min), 95% ethanol (6 min), 85% ethanol (6 min), and 75% ethanol (5 min), followed by rinsing in running water. Slides were stained with hematoxylin for 3–8 min, washed in tap water, briefly differentiated with 1% hydrochloric acid alcohol, and counterstained with eosin for 1–3 min. Dehydration and clearing were performed sequentially in 75% ethanol (30 s), 85% ethanol (30 s), 95% ethanol (1 min), 95% ethanol II (2 min), 100% ethanol II (5 min), 1:1 mixture of dimethylbenzene and ethanol (5 min), and dimethylbenzene II (5 min). Sections were air-dried and mounted with coverslips for microscopic examination and image capture.

Immunostaining and quantification of testicular tissues

Prepared paraffin sections of testicular tissue were deparaffinized and rehydrated in a xylene series (I, II, xylene: alcohol=1:1, 20 min each), followed by an ethanol series (100%, 95%, 85%, 75%, 10 min each) and rinsing in distilled water (3 min, twice). Antigen retrieval was performed in Tris-EDTA solution (pH 9.0, 0.05% Tween-20) in a hot water bath (95–98°C) for 30 min. Sections were allowed to cool naturally and washed in PBS containing 0.2% Tween-20 (PBS-T) three times (5 min each). Permeabilization was performed using PBS with 0.05% Triton X-100 for 20 min. Immunohistochemical detection was performed using the PV-9000 universal two-step detection system (Beijing Zhongshan Jinqiao Biotechnology, China).

For immunofluorescence, sections were first incubated with 10% FBS at RT for 30 min, followed by incubation with primary antibodies diluted in NCM universal antibody diluent (Supplementary Table S1) overnight at 4°C in a humidified chamber. After rinsing with PBS three times (3 min each), Alexa Fluor 488-conjugated goat anti-rabbit secondary antibody was applied dropwise and incubated at RT for 1 h. Sections were again washed with PBS three times (3 min each) and counterstained with 4',6-diamidino-2-phenylindole (DAPI). The sections were then observed and photographed after the blocking step.

Images were captured using an Eclipse Ti2-E fluorescence microscope (Nikon, Japan), and each target antigen was imaged in multiple non-overlapping fields. Quantification was performed using ImageJ v.1.54f Antigen expression levels were represented as average optical density for immunohistochemistry and relative fluorescence intensity for immunofluorescence.

ScRNA-seq data analysis

The Cell Ranger output files (barcode.tsv, features.tsv, and matrix.mtx) were imported into R using the “Read10X” function in the Seurat package (https://satijalab.org/seurat/, R package v.4.3.0). Individual Seurat objects were created using initial filtering thresholds (minimum 200 genes per cell; each gene expressed in at least 100 cells). The two Seurat objects were then merged. Cells were retained if they expressed between 1 000 and 6 000 genes and had a $\log_{10}$(GenesPerUMI)>0.8. After filtering, 6 800 cells from the *Brucella*-infected testis and 8 379 cells from the normal testis were included. Normalization was performed using the “LogNormalize” method. Highly variable genes (top 4 000) were identified with the “FindVariableFeatures” function. Samples were integrated using Harmony (Korsunsky et al., 2019) to remove batch effects and select the first 50 dimensions for analysis. Uniform manifold approximation and projection (UMAP) and clustering analyses were performed on the combined data using the top 4 000 highly variable genes and principal components (PCs) 1–50, with a resolution parameter of 0.5. Cell type annotation was conducted based on the Seurat tutorial.

Identification of DEGs associated with brucellosis

Brucellosis-associated DEGs were identified by comparing gene expression profiles between *Brucella*-infected and control goat testicular samples using the “FindMarkers” function in Seurat. Genes with expression level differences greater than 0.25, min.pct=0.25, and *P*_adjust values less than 0.01 were set as the DEG threshold. DEGs in different samples were analyzed using an unpaired two-sided Student’s *t*-test. Statistical significance was set at $P<0.05$. Gene Ontology (GO) enrichment analysis of brucellosis-associated DEGs was performed using the DAVID online annotation platform.

T cell pseudotime trajectory analysis

Pseudotime trajectory inference of T cell subsets was performed using the Monocle2 package (v.2.34.0) (Qiu et al., 2017) with default settings. Ordering genes were identified using the differential "GeneTest()" function with a threshold of *Q*val<0.01. Discriminative dimensionality reduction with trees (DDRTree) was used to reduce data to two dimensions. T cell pseudotime trajectory was visualized using the “plot_cell_trajectory()” function. Identified gene sets were clustered and visualized using the “plot_pseudotime_heatmap()” and “plot_genes_in_pseudotime()” functions.

Analysis of cell-cell communication networks

Due to the absence of curated goat-specific ligand-receptor libraries, goat genes in the single-cell matrix were mapped to their human homologs using the “getLDS” function in the biomaRt package. A total of 10 597 homologous genes were retained to construct the expression matrix for downstream analysis. Cell-cell communication networks were inferred using the CellChat R package (v.1.6.0, https://github.com/sqjin/CellChat) (Jin et al., 2021), with “CellChatDB.human” used as the reference ligand-receptor interaction database. CellChat objects were constructed for each condition using default parameters and visualized using the built-in plotting functions. To enable direct comparison of signaling networks, CellChat objects were merged using the “mergeCellChat” function, and differences in interaction quantity and strength were assessed. Comparative signaling pathway sharing among groups was determined using the “rankNet” function.

Weighted gene co-expression network analysis (WGCNA)

To identify hub genes in specific testicular cell populations—

including T cells, macrophages, NR2F1$^+$ endothelial cells, and Sertoli cells—WGCNA was performed using the WGCNA R package (v.1.72) (Langfelder & Horvath, 2008). To reduce noise and outlier effects in the single-cell datasets, pseudo-cells were constructed by aggregating random groups of 10 cells from the same cell type. These pseudo-cell expression profiles were combined with the top 6 000 hypervariable genes to generate the input matrix. An unsigned co-expression network was built using Pearson correlation with default soft-thresholding to approximate scale-free topology. Module-trait relationships were evaluated based on Pearson correlation coefficients and corresponding *P*-values. Module quality was confirmed by assessing the correlation between module eigengenes and traits of interest, as well as the correlation between gene module membership and gene-trait correlation. Hub genes (top 30) from each key module were selected based on the top 100 genes with the highest intramodular connectivity (sum of in-module edge weights). Network visualizations were generated using Cytoscape (v.3.9.1) (Otasek et al., 2019).

Regulon analysis

Following homologous mapping of goat genes to their human counterparts, regulon analysis of testicular cell populations was conducted using pySCENIC (v.0.12.1) within a Linux Docker environment. PySCENIC is a combination of three packages: GENIE3, RcisTarget, and AUCell. We performed regulon analysis following the tutorials provided by pySCENIC (https://github.com/aertslab/pySCENIC/)(Van de Sande et al., 2020).

Genes available in human feather databases (hg38_refseq-r80_500bp_up_and_100bp_down_tss.mc9nr.genes_vs_motifs.rankings.feather,hg38_refseq-r80_10kb_up_and_down_tss.mc9nr.genes_vs_motifs.rankings.feather) are utilized. The final output included a specificity score matrix comprising 888 regulons, which was visualized in R. Transcription factor binding motifs were further examined using the JASPAR database (https://jaspar.genereg.net/).

RESULTS

Single-cell transcriptomic profiling of normal and *Brucella*-infected goat testes

To investigate testicular immune alterations in response to *Brucella* infection, a portion of the testicular tissue from a 6-year-old confirmed to be *Brucella*-positive via the Rose-Bengal plate agglutination test (Supplementary Figure S1B) was subjected to scRNA-seq using the 10x Genomics Chromium platform. The resulting dataset was integrated with a previously published scRNA-seq dataset from normal goat testes (Yu et al., 2021) for comparative analysis (Figure 1A). Histopathological examination revealed pronounced structural divergence between normal and infected testes (Figure 1C). In the normal testis, seminiferous tubules exhibited intact spermatogenic architecture, with ordered germ cell layers and intact Sertoli cells, confirming active spermatogenesis. In contrast, *Brucella*-infected tissue exhibited severe spermatogenic disruption, characterized by marked thinning and disorganized cell layers of the germinal epithelium, vacuolated Sertoli cell cytoplasm, and interstitial infiltration of blood cells (Figure 1C; Supplementary Figure S2B), consistent with previous reports (Hassaneen et al., 2024; Yu et al., 2022).

Post-quality control, integration of both datasets yielded a total of 15 179 single cells, with per-cell read depths ranging from 5 000–50 000 and counts spanning 1 000–6 000. UMAP was performed using Seurat and Harmony, identifying 12 transcriptionally distinct clusters, subsequently annotated using canonical markers (Figure 1B; Supplementary Figures S1C, S2A). Testicular cells were broadly classified into testicular spermatogenic and somatic cells (Figure 1B). The spermatogenic cells were further subdivided into Meiosis-I (*FKBP6*, *SYCP2*), Meiosis-II (germ cells that do not enter sperm differentiation; *LCA5*, *ACRV1*^{low}), round spermatids (*ACRV1*^{high}, *ACTL7B*), elongating spermatids (*SEL1L2*, *HEMGN*), and mature sperm (*SPEM1*, *TNP1*) (Supplementary Figure S1C). Somatic cells were further divided into Sertoli cells (SC, *SOX9*, *AMH*), Sertoli progenitor cells (SPC, *INHA*, *PLAC1*), immature Leydig and peritubular myoid cells (Immature LC & PMC, *IGFBP6*, *ACTA2*, *MYH11*), perivascular niche cells (PNC, *CD34*, *VWF*, *IGFBP7*), NR2F1$^+$ endothelial cells (NR2F1+ EC, *NR2F1*, *PECAM1*), T cells (*CD8A*, *CD3E*), and macrophages (*CD74*, *C1QA*) (Figure 1D). GO analysis of DEGs confirmed cell-type assignment (Supplementary Figure S1D).

Developmental dynamics of the spermatogenic lineage were reconstructed using pseudotime trajectory analysis with Monocle, which revealed a progression consistent with known stages of spermatogenesis (Supplementary Figure S2C–E). Notably, cell-type distribution was skewed between conditions, with germ cells predominately derived from the normal testis, while the *Brucella*-infected sample exhibited enrichment of T cells, NR2F1$^+$ endothelial cells, and Sertoli cells (Supplementary Figure S1A). However, quantitative analysis of SOX9-positive cells within seminiferous tubules demonstrated no significant difference in Sertoli cell number between conditions (Supplementary Figure S3A, B). These findings suggest that *Brucella* infection induces substantial alterations in the testicular immune microenvironment, particularly within adaptive immune and vascular compartments, warranting deeper dissection of cell-type-specific heterogeneity and infection-associated transcriptional remodeling.

Up-regulated pathways in somatic cell populations associated with brucellosis

To elucidate the impact of *Brucella* infection on the somatic testicular environment, transcriptional profiles were compared across somatic cell types between infected and control samples (Figure 2A). In total, 723 genes were up-regulated and 1 554 were down-regulated, with most showing cell-type specificity. However, subsets of up-regulated genes were shared across multiple somatic populations, with 26 genes detected in more than two cell types and 105 genes detected between two cell types, suggesting conserved immunopathological responses. Functional enrichment analysis of shared up-regulated genes revealed overrepresentation of immune-related GO terms, including “B cell differentiation” and “response to bacterium”. Several immune regulatory genes exhibited coordinated up-regulation across somatic populations. *EP300*, a transcription factor associated with B cell activation, was elevated in two somatic cell types (Hashwah et al., 2017; Sandberg et al., 2005). *TXNIP*, a pro-inflammatory regulator known to activate the NLRP3 inflammasome and promote oxidative stress–induced apoptosis (Zhan et al., 2022; Hu et al., 2020), showed up-

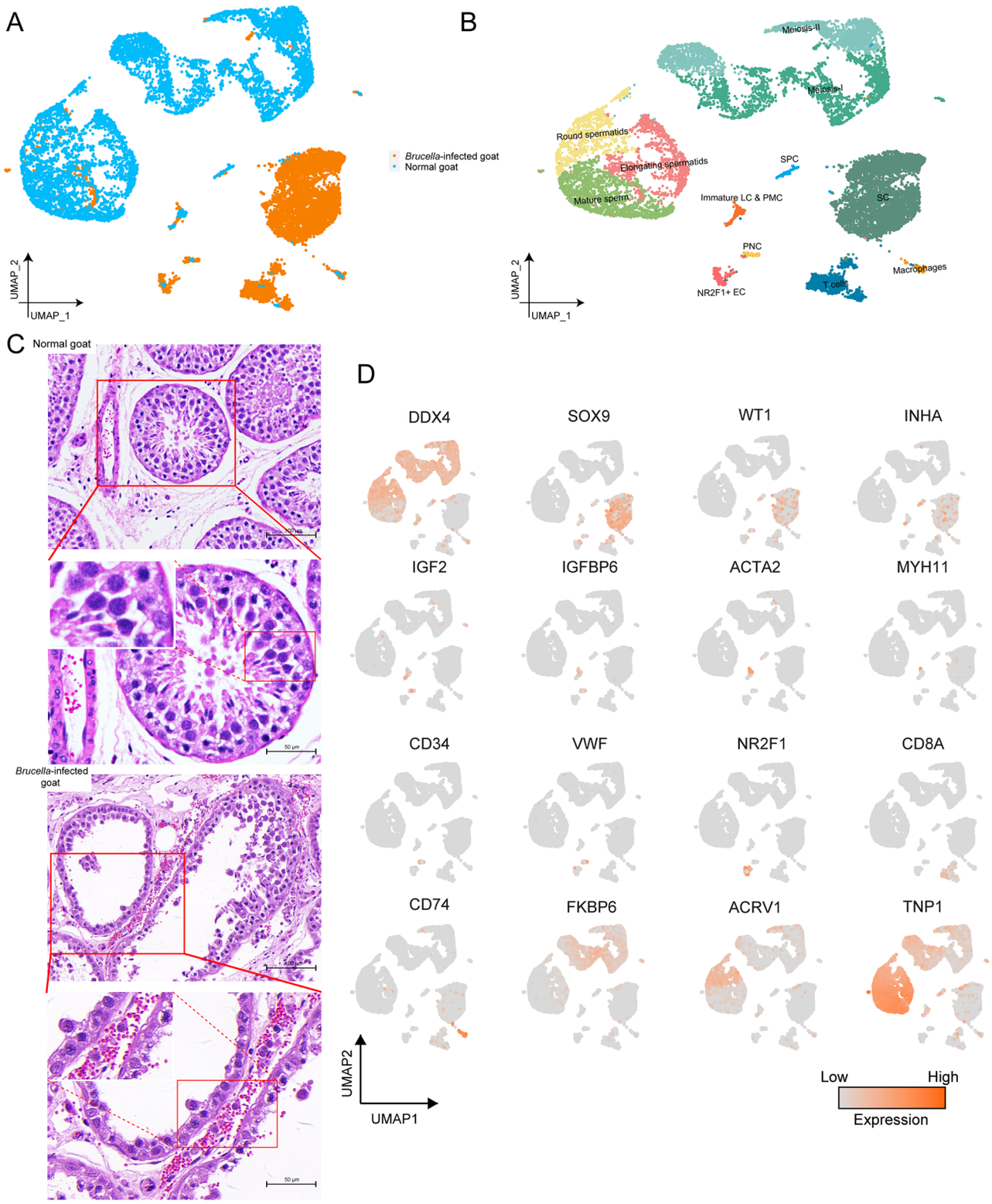

Figure 1 Single-cell transcriptomic profiling of normal and *Brucella*-infected goat testes

A: UMAP visualization of integrated single-cell transcriptomic data from normal and *Brucella*-infected goat testes (*n*=15 179). Each dot represents a single cell and is colored according to its donor of origin. B: UMAP plot from panel A, labeled with corresponding cell type identities and colored accordingly. C: Hematoxylin and eosin (H&E) staining of representative testis sections illustrates morphological alterations associated with *Brucella* infection. Normal testis: Low magnification (scale bar: 100 μm) showing multiple seminiferous tubules (STs) with normal spermatogenesis; high magnification inset (scale bar: 50 μm) highlighting detailed structure of seminiferous epithelium. *Brucella*-infected testis: Low magnification (scale bar: 100 μm) showing multiple STs with impaired spermatogenesis; high magnification inset (scale bar: 50 μm) showing interstitial inflammatory infiltration and rare immune cells, as confirmed by CD45 immunostaining in Supplementary Figure S4C. D: Expression of representative marker genes projected onto the UMAP plot in panel B, with one or two markers shown per cell cluster.

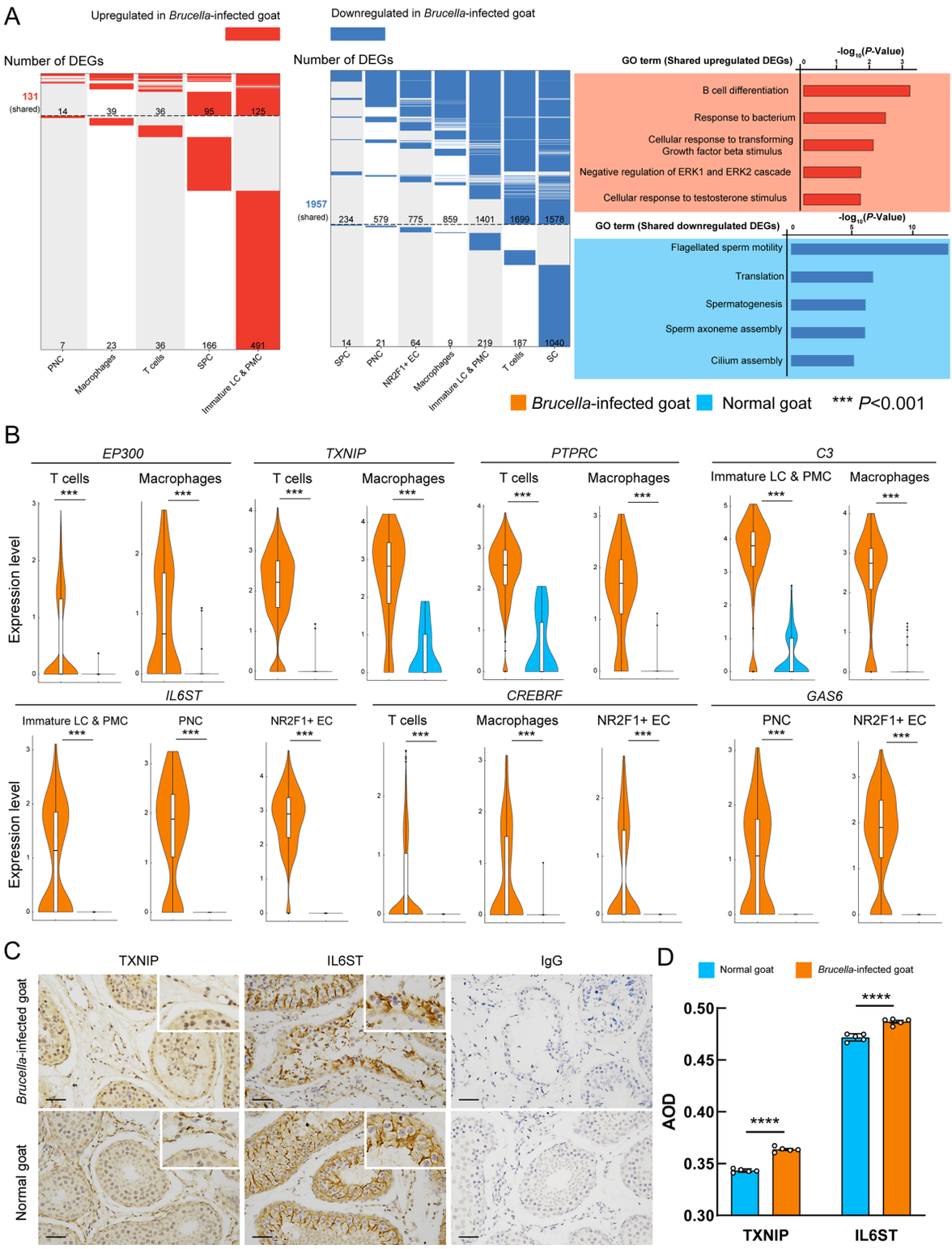

Figure 2 Cell-specific up-regulated pathways in somatic cell populations associated with brucellosis

A: Left and middle panels: heatmap showing shared and distinct up-regulated (left) and down-regulated (middle) DEGs in major testicular somatic cell types between *Brucella*-infected and normal goats. Right panel: representative Gene Ontology (GO) terms associated with shared up-regulated (top) and down-regulated (bottom) DEG, along with corresponding *P*-values. B: Violin plots showing representative up-regulated DEGs in testicular somatic cells from *Brucella*-infected goats. Boxes within violins indicate mean expression levels. C: Immunohistochemical staining of TXNIP and IL6ST (brown) showing increased expression in *Brucella*-infected goat testis compared to normal testis, where staining is comparatively weak. TXNIP localized primarily to interstitial regions, while IL6ST exhibited dominant expression in Sertoli cells, as indicated by morphological characteristics and staining patterns. Nuclei were counterstained with hematoxylin (blue). No signal was detected in IgG controls. Scale bars: 50 μm. D: Quantification of TXNIP and IL6ST expression by average optical density (AOD) in Brucella-infected and normal goat testes. Data are presented as mean±standard deviation (SD) and represent five independent visual fields. ns: Not significant; *: $P<0.05$; **: $P<0.01$; ***: $P<0.001$; ****: $P<0.0001$ (two-tailed *t*-test).

regulation in five somatic subsets (Supplementary Figure S2F). *PTPRC* (CD45), a critical mediator of antigen receptor signaling in T and B cells through interactions with receptor-associated components and activation of Src family kinases (Jung et al., 2021), was up-regulated in two somatic cell populations. Additionally, *C3*, a key component of complement activation (Lamers et al., 2022), was shared by two somatic cell types. Within NR2F1^{+} endothelial cells, *IL6ST* (gp130), the signal-transducing β subunit of the IL-6 receptor complex (IL6R/IL6ST) (Osman & Neamati, 2024), was highly expressed in *Brucella*-infected samples, suggesting a potential role in modulating downstream immune signaling. Additional factors included *CREBRF*, a negative regulator of endoplasmic reticulum stress and the unfolded protein response (Audas et al., 2008; Wang & Kaufman, 2016), and *GAS6*, a mediator of cell adhesion and migration (Shibata et al., 2020; Wu et al., 2018) (Figure 2B). Notably, the expression levels of *EP300*, *TXNIP*, *PTPRC*, *C3*, *IL6ST*, *CREBRF*, and *GAS6* were up-regulated in *Brucella*-infected testis compared to normal testis samples, supporting the hypothesis that brucellosis-associated genes involved in adaptive immune regulation are key drivers of disease progression.

Quantitative analyses confirmed the transcriptional findings. Immunohistochemistry and immunofluorescence revealed elevated TXNIP expression in *Brucella*-infected testes relative to controls (Figure 2C, D; Supplementary Figure S4A, B). Similarly, IL6ST immunostaining demonstrated enhanced signal intensity in infected tissue (Figure 2C, D), and CD45 expression was significantly increased (Supplementary Figure S4C, D), suggesting that *Brucella* infection drives widespread activation of adaptive immune signaling across somatic cell types.

GO analysis of down-regulated genes shared across somatic populations revealed strong enrichment for processes related to spermatogenesis, including “flagellated sperm motility”, “spermatogenesis”, “sperm axoneme assembly”, and “cilium assembly” (Figure 2A). ZO-1 staining of tight junctions within the seminiferous epithelium indicated complete blood-testis barrier disruption in infected samples (Supplementary Figure S4E, F), consistent with histological observations of reproductive disruption.

Together, these findings demonstrate that Brucella infection induces convergent transcriptional responses among somatic cell types characterized by immune activation, cytokine signaling, and stress adaptation, while simultaneously disrupting germline support and barrier integrity—highlighting a mechanistic link between somatic immune remodeling and impaired testicular function.

T cell state transitions and activation dynamics in *Brucella*-infected testis

To characterize T cell responses during *Brucella* infection, a focused single-cell analysis was conducted on 1 055 T cells extracted from the infected testis. Reclustering identified three transcriptionally distinct subpopulations (Figure 3A). Pseudotime trajectory analysis resolved these cells into three temporal states, capturing dynamic transitions across the activation landscape (Figure 3B). Temporal clustering of gene expression along the pseudotime axis yielded five major gene clusters (Figure 3C). Cluster C1, comprising 1 259 genes, was predominantly expressed in early-state T cells and enriched for biological processes related to “microtubule cytoskeleton organization”, “small GTPase-mediated signal transduction”, “fatty acid beta-oxidation”, “mitochondrial respiratory chain complex I assembly”, and “protein localization to plasma membrane”. Cluster C4, containing 200 genes, exhibited a similar early-stage pattern and was associated with mRNA transcriptional regulation. The expression trajectories of C1 and C4 suggest that early-stage T cells undergo metabolic priming and transcriptional reprogramming to support adaptive immune responses, consistent with previous reports (Hunt et al., 2024; Lopes et al., 2021; Xu et al., 2021).

UMAP projection of representative genes highlighted transcription factors such as ZFHX3 (Liu et al., 2024b), EPAS1 (Schönenberger et al., 2015), and KLF16 (Ma et al., 2022), as well as genes linked to vesicular trafficking and mitochondrial function, including *BCAR3*, *GDI2*, *NDUFS8*, *NDUFAF6*, and *TSPAN5* (Colbert et al., 2022; Sung et al., 2024; Yin et al., 2024). *RAMP1*, involved in CGRP-RAMP1-mediated immune modulation (Kulalert et al., 2024), also showed coordinated expression during this phase. Remarkably, genes in clusters C2, C3, and C5 were significantly up-regulated toward the terminal pseudotime state (State 3) (Figure 3C). GO enrichment analysis of these late-stage clusters revealed functional associations with “positive regulation of T cell mediated cytotoxicity”, “integrin-mediated signaling pathway”, “T cell receptor signaling pathway”, and “positive regulation of natural killer cell-mediated cytotoxicity”, suggesting that T cells are in a highly activated state at this stage. Expression trajectories of representative genes across the pseudotime continuum further corroborated this transition (Figure 3D).

Together, these results define a dynamic progression of T cell activation during Brucella infection, marked by early metabolic and transcriptional priming followed by robust acquisition of effector functions aligned with adaptive cytotoxic responses.

Global alterations in cells in *Brucella*-infected testis

To explore global alterations in testicular intercellular signaling in *Brucella*-infected samples, CellChat analysis was conducted. Results revealed marked increases in both the number and intensity of signaling interactions in *Brucella*-infected testis compared to healthy controls (Figure 4A, C). Clustering of communication patterns identified four major signaling modules (Figure 4B), with a prominent cluster (purple) encompassing immune-associated pathways, including MIF, GAS, CXCL, PORS, and SEMA7. Notably, GAS, CXCL, PORS, and SEMA7 signaling pathways were uniquely observed in the infected testis, indicating pathogen-specific activation of immunomodulatory circuits.

Across the global signaling landscape, 42 ligand-receptor pathways were detected, with 13 shared between *Brucella*-infected and normal conditions (LAMININ, CDH5, PTPRM, CDH, CD45, APP, MIF, CADM, GRN, PTN, NECTIN, JAM, CD39) (Figure 4D). Immune-somatic interactions were markedly intensified in the infected sample, particularly involving macrophages and T cells. For example, CD45-mediated signaling from immune cells and somatic populations was significantly elevated in the *Brucella*-infected testis (Figure 4F; Supplementary Figure S4C, D). Given that CD45 dephosphorylates negative regulatory sites on Src family kinases to enable T cell receptor signaling (Jung et al., 2021), this enhancement confirmed the importance of adaptive immunity in *Brucella* removal. Furthermore, somatic-

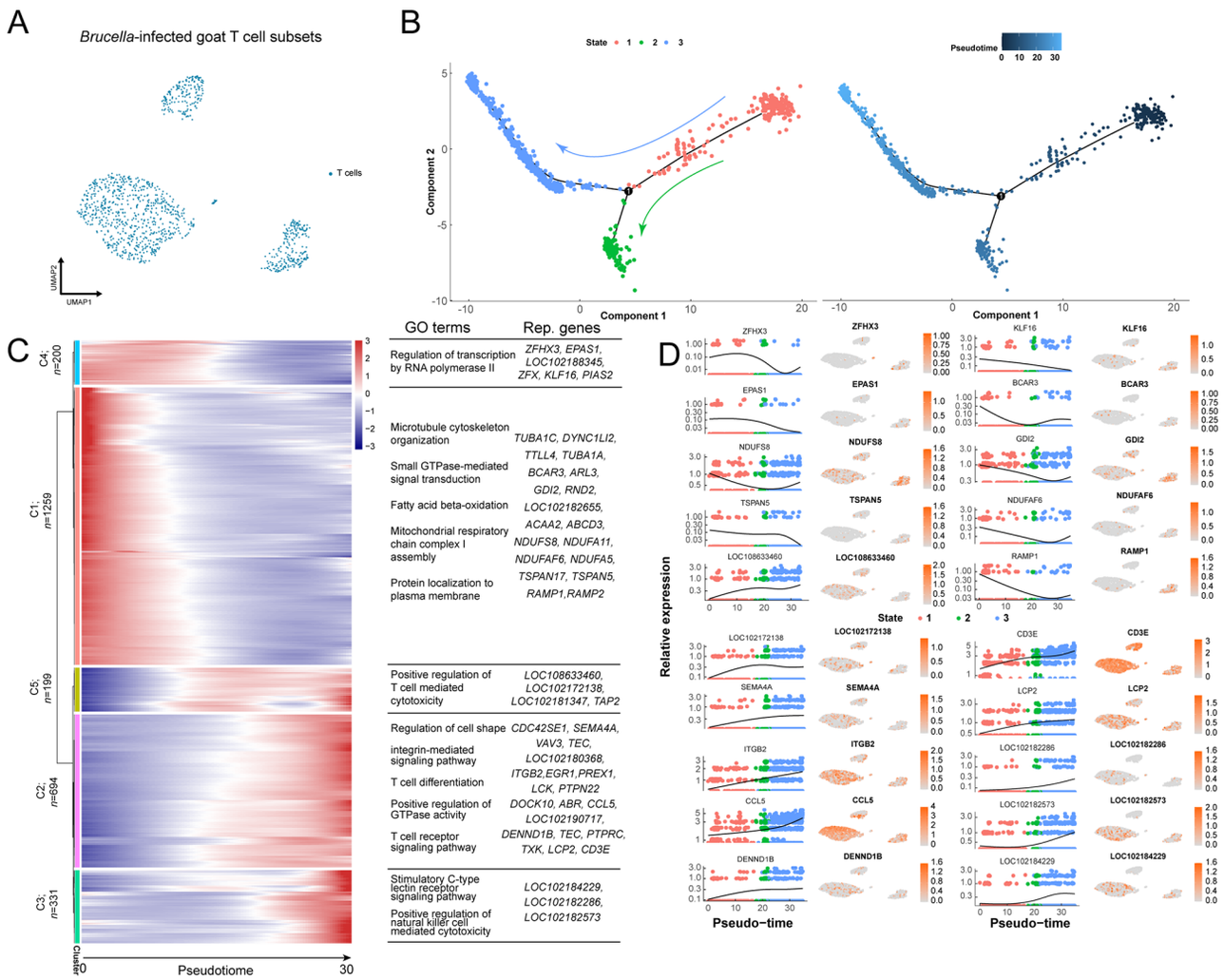

Figure 3 Dynamic transcriptional changes in T cells from *Brucella*-infected goat testes

A: UMAP projection of T cells from *Brucella*-infected goat testis, highlighting major subpopulations. B: Pseudotime trajectory of T cells reconstructed using Monocle, with distinct cell states indicated by different colors. C: K-means clustering of 2 683 pseudotime-associated DEGs. Each row represents a gene and each column represents a single cell. Z-scored expression levels are shown by color intensity. Representative GO terms associated with each gene cluster were annotated using DAVID. Rep. genes: Representative genes. D: Expression patterns of selected genes projected onto the UMAP plot (panel A) and mapped across three pseudotime-defined cell states.

to-macrophage signaling through MIF was increased, consistent with its established role in regulating macrophage activity in host defense (Sumaiya et al., 2022). In contrast, the CD39 signaling pathway, implicated in maintaining testicular immune privilege (Jenabian et al., 2016; Takenaka et al., 2016; Zhao et al., 2014), was decreased following *Brucella* infection (Figure 4F; Supplementary Figure S3E, F).

Receptor-ligand pair analysis further highlighted the mechanistic basis of *Brucella*-induced immunomodulation. Macrophages and T cells engaged in paracrine and autocrine signaling with somatic and germ cell populations (Figure 4E). Notably, PTPRC (CD45)-MRC1 signaling was elevated in both immune cell types in the *Brucella*-infected testis, consistent with prior observations. MIF-CD74/CD44 and ITGB2-ICAM interactions were also elevated in the infected samples. Conversely, JAM3-JAM2 and JAM3-F11R interactions within the junctional adhesion molecule (JAM) pathway were down-regulated following infection (Supplementary Figure S3C, D, G, H), suggesting a potential role of this pathway in maintaining the blood-testis barrier (Wang & Cheng, 2007; Yan & Cheng, 2005; Yan et al., 2008).

These findings collectively indicate that Brucella infection reconfigures the testicular signaling landscape in a manner that amplifies immune activation while potentially compromising germline protection.

WGCNA identifies hub genes during *Brucella* infection

To investigate potential disease-resistant genes, WGCNA was performed on single-cell transcriptomic data, yielding a co-expression network constructed from the top 6 000 highly variable genes. Hierarchical clustering segregated these genes into six distinct modules based on shared expression dynamics (Figure 5A). The green module displayed the strongest positive correlation with T cells and macrophages (ME=0.83, P=0) and the strongest negative correlation with meiotic stage II (ME=− 0.24, P=9e−21) (Figure 5B). The blue module exhibited the strongest positive correlation with Sertoli cells (ME=0.92, P=0) and the strongest negative association with meiotic stage II (ME=−0.39, P=3e−56). The gray module displayed the strongest positive correlation with NR2F1$^+$ endothelial cells (ME=0.85, P=0).

Subnetwork construction using Cytoscape and ranking by degree (node connectivity) and edge weight (gene

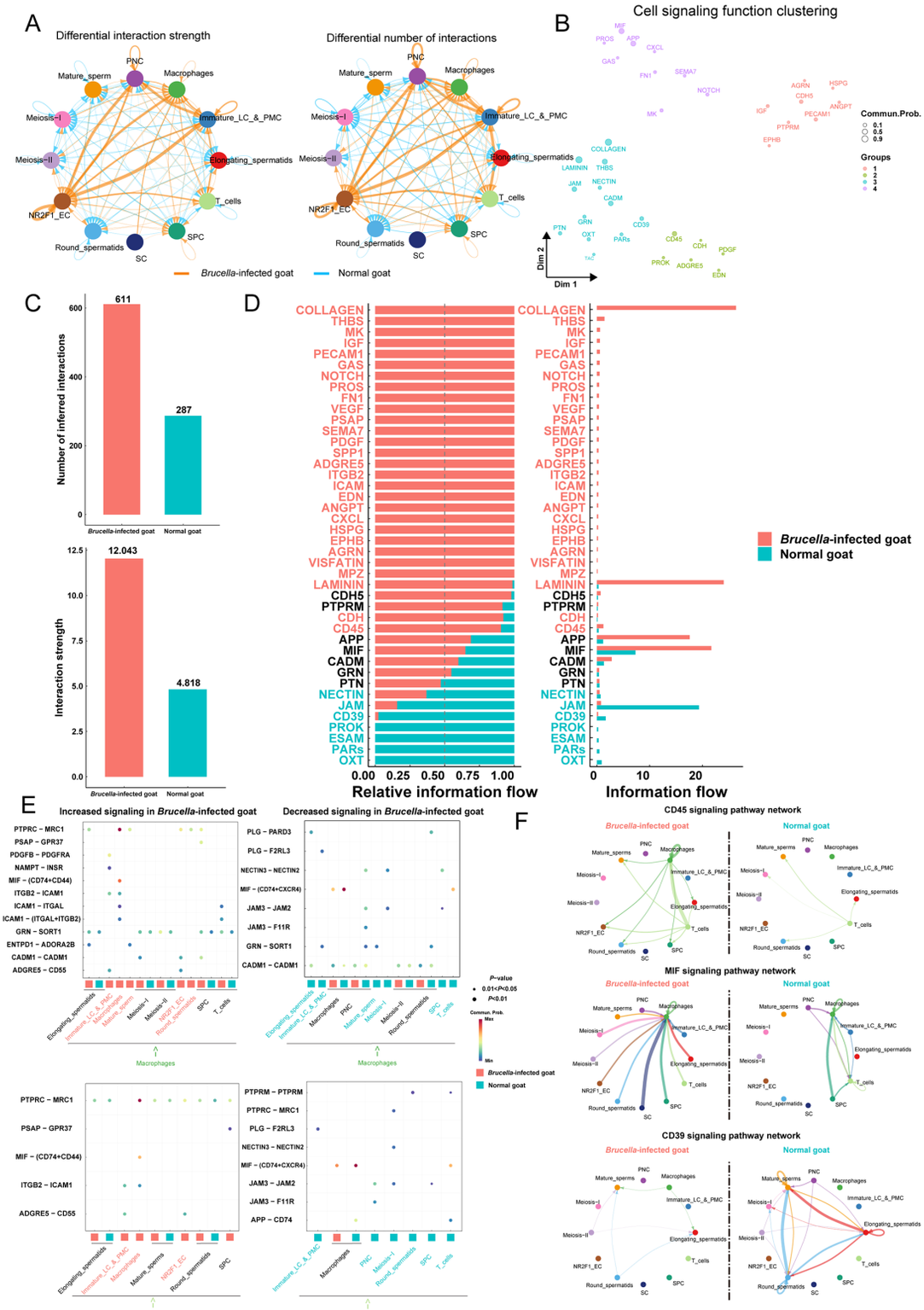

Figure 4 Global alterations in testicular cell-cell communication networks between *Brucella*-infected and normal goats

A: Total number and overall strength of inferred intercellular interactions among all testicular cell types in *Brucella*-infected and normal goats. B: Two-dimensional projection of signaling pathways based on functional similarity. Each dot represents the communication network of one signaling pathway; dot size is proportional to the overall communication probability. Different colors represent different signaling pathway groups. Commun.Prob.: Communication probability. C: Bar graphs comparing number (top) and strength (bottom) of inferred ligand-receptor interactions between groups, as analyzed using CellChat. D: Overall information flow of individual signaling pathways in *Brucella*-infected and normal goats. E: Visualization of increased and decreased signaling in *Brucella*-infected goat via ligand-receptor interactions of T cells and macrophages (P<0.05). Circle size indicates P-value, with red denoting communication probability; square color indicates sample source, with turquoise for normal goat and red for *Brucella*-infected goat. F: Circle plots of selected differential signaling networks. Edge width indicates communication probability, and edge color denotes sample origin (turquoise: Normal; red: Infected).

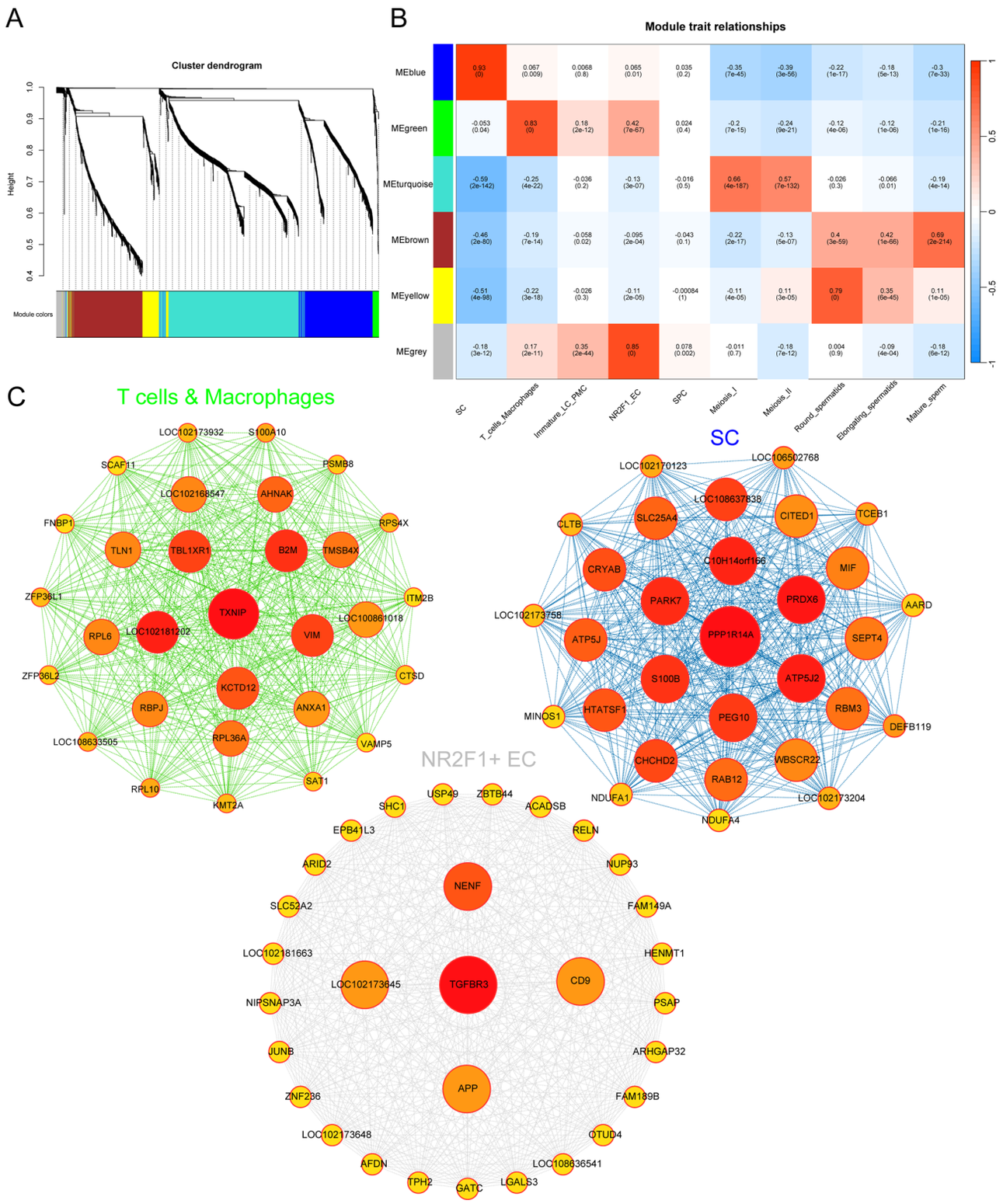

Figure 5 WGCNA reveals key immune-related hub genes

A: Hierarchical clustering dendrogram of 6 000 variable genes constructed using a dissimilarity measure. Genes with high correlation were grouped into distinct co-expression modules, each represented by a unique color. B: Heatmap showing correlations between module eigengenes and 10 major testicular cell types. Each cell presents the correlation coefficient and corresponding *P*-value. C: Visualization of gene co-expression networks showing top 30 hub genes within the green, gray, and blue modules. Red represents core hub genes.

association) identified key hub genes in each module (Figure 5C). In the green module, *TXNIP* emerged as the central hub gene within macrophage and T cell-associated networks, corroborating earlier observations (Figure 2C; Supplementary Figure S4A). Prior studies have demonstrated that *Brucella* infection induces TXNIP degradation via the regulated IRE1-dependent decay (RIDD) pathway (Wells et al., 2022), and that loss of TXNIP in RAW264.7 macrophages facilitates intracellular proliferation of *Brucella abortus* (Hu et al., 2020). In the present dataset, TXNIP-

expressing cells were extracted for GO enrichment analysis, revealing functional enrichment for Notch-mediated endothelial repair and adaptive immune activation (Supplementary Figure S4G–I). Other hub genes in the green module included *B2M*, *TBL1XR1*, *VIM*, *KCTD12*, and *LOC102181202* (MHC-I, BOLA class I histocompatibility antigen, alpha chain BL3-7). Within the Sertoli cell-enriched blue module, hub genes included *PPP1R14A*, *C10H14orf166* (*RTRAF* [*Homo sapiens*]), *PRDX6*, *ATP5J2*, *PEG10*, *S100B*, and *PARK7*. Notably, *PPP1R14A* (*CPI-17* [*Homo sapiens*]), a known inhibitor of PPP1CA, belongs to the protein phosphatase 1 (PP1) family and regulates intracellular phosphorylation events, thereby influencing various biological processes (Eto, 2009; Yang et al., 2018). Mitochondrial regulators such as *ATP5J2*, *PRDX6*, and *PARK7* (Chen et al., 2024b; Danileviciute et al., 2022; Galber et al., 2021) were also prominent. Furthermore, *TGFBR3* was identified as a central hub gene in the NR2F1$^+$ endothelial cell network, highlighting the significant role of TGFβ signaling in response to *Brucella* infection.

Together, these findings identify potential anti-disease target molecules, providing valuable evidence for *Brucella* resistance breeding and advancing our understanding of how *Brucella* influences host immune regulation.

Gene regulatory network analysis reveals cell-type-specific transcriptional control during *Brucella* infection

To systematically dissect regulatory hierarchies underlying cellular responses to *Brucella* infection, single-cell transcriptomic data were analyzed using the pySCENIC pipeline to infer regulon activity across diverse testicular cell types (Van de Sande et al., 2020). Regulon specificity scores (RSS) identified transcriptional modules with enriched activity in specific populations, and the top 10 regulons for each lineage were visualized using cell-type-resolved UMAP plots (Figure 6A, D, F, I). T cell and macrophage populations exhibited distinct activation of *SEMA4A*, *HCLS1*, *ELF1*, and *GATA3* regulons, with spatial restriction confirmed by expression projection on UMAP plots (Figure 6B, E, G, J). These findings were further corroborated by UMAP visualization, which demonstrated that these regulons exhibited highly specialized activity in T cells and macrophages. Notably, all four factors are well-known master regulators for T cells and macrophages (Ji et al., 2002; Naito et al., 2023; Shin et al., 2012; Wan, 2014). Moreover, GATA3 was also found to be highly expressed in the *Brucella*-infected samples (Supplementary Figure S5A, B).

Further analysis revealed cell-type-specific regulatory signatures across both immune and non-immune lineages. In macrophages, *ZNF366*, *IRF5*, *NFKB1*, *SPI1*, and *ETV6* represented the most active regulons, consistent with their known roles in macrophage activation and differentiation (Lawrence & Natoli, 2011; Villar et al., 2023a, 2023b; Zhang et al., 2024). In T cells, transcriptional control was dominated by *TCF7*, *SATB1*, *BCL11B*, *ID2*, and *RBPJ*, key mediators of T cell lineage commitment and function (Chen et al., 2019; Pais Ferreira et al., 2020; Trujillo-Ochoa et al., 2023). Immunostaining confirmed that IRF5 protein levels were significantly elevated in infected samples (Supplementary Figure S5C, D), corroborating the transcriptional data. Within NR2F1$^+$ endothelial cells, *ZNF521*, *MEIS2*, *TCF7L1*, and *NR2F1* regulons were specifically enriched. *TCF7L1* (*TCF3* [*Homo sapiens*]), a known Wnt pathway effector, has been implicated in endothelial cell differentiation and morphogenesis (Athanasouli et al., 2023; Nguyen et al., 2006). In elongating spermatids, *SP5*, *MRPS25*, and *MRPL2* were the top regulators. SP5 is a negative regulator of the Wnt signaling pathway (Huggins et al., 2017), while MRPS25 and MRPL2 are associated with mitochondrial protein synthesis (Cheong et al., 2020; Zou et al., 2021), highlighting a convergence of transcriptional and metabolic control during spermatogenesis. Transcription factor binding motif analysis using the JASPAR database revealed distinct motif landscapes for each lineage, further supporting cell-type specificity of the identified regulatory programs (Figure 6K).

To assess broader regulon co-regulation patterns, 888 regulons were hierarchically clustered and subjected to GO enrichment analysis (Figure 6C, H). Cluster C7 was predominantly associated with immune cell development and differentiation. Cluster C8, highly active in Sertoli cells, was significantly enriched for terms linked to “male sex differentiation”, “development of primary male sexual characteristics”, and “male gonad development”. Clusters C1, C2, and C4 were enriched in non-spermatogenic somatic cells and negatively associated with DNA replication and RNA transcription pathways.

Together, these data delineate a multilayered regulatory atlas of cell identity and infection-induced remodeling within the testis, revealing key transcriptional circuits that govern immune activation, somatic cell function, and germline development during Brucella infection.

DISCUSSION

Brucella infection exerts profound effects on testicular architecture and immune regulation, with significant implications for global livestock production as well as human health due to its zoonotic potential (De Bolle et al., 2015; Qureshi et al., 2023; Yu et al., 2022). However, the molecular mechanisms underlying its pathogenesis and effects on goat immunity remain poorly understood. Here, single-cell transcriptomic profiling of healthy and infected goat testes revealed extensive remodeling of germline and somatic compartments, accompanied by pronounced activation of innate and adaptive immune pathways. Histological and molecular analyses confirmed severe disruption of seminiferous tubule organization and loss of blood-testis barrier integrity in infected samples, consistent with diminished ZO-1 expression (Supplementary Figure S4E, F) and down-regulation of JAM3 and CD39 signaling (Supplementary Figure S3C–H). Aligning with histopathological observations, CD45, GATA3, and IRF5 showed up-regulated expression, indicating immune cell infiltration (Supplementary Figures S4C, D, S5A–D). WGCNA and differential gene expression analysis identified key transcriptional changes in host cells during *Brucella* infection, with TXNIP emerging as a critical regulator of the cellular response to pathogen invasion. This finding aligns with previous evidence implicating TXNIP in oxidative stress-mediated pathways that influence both bacterial pathogenesis and immune regulation (Hu et al., 2020). Future investigation into TXNIP may support the development of targeted immunomodulatory strategies to strengthen host defense against *Brucella*. Longitudinal studies with larger sample sizes would provide deeper insights into the temporal dynamics of these immune responses during the course of infection.

Pseudotime trajectory analysis revealed three distinct

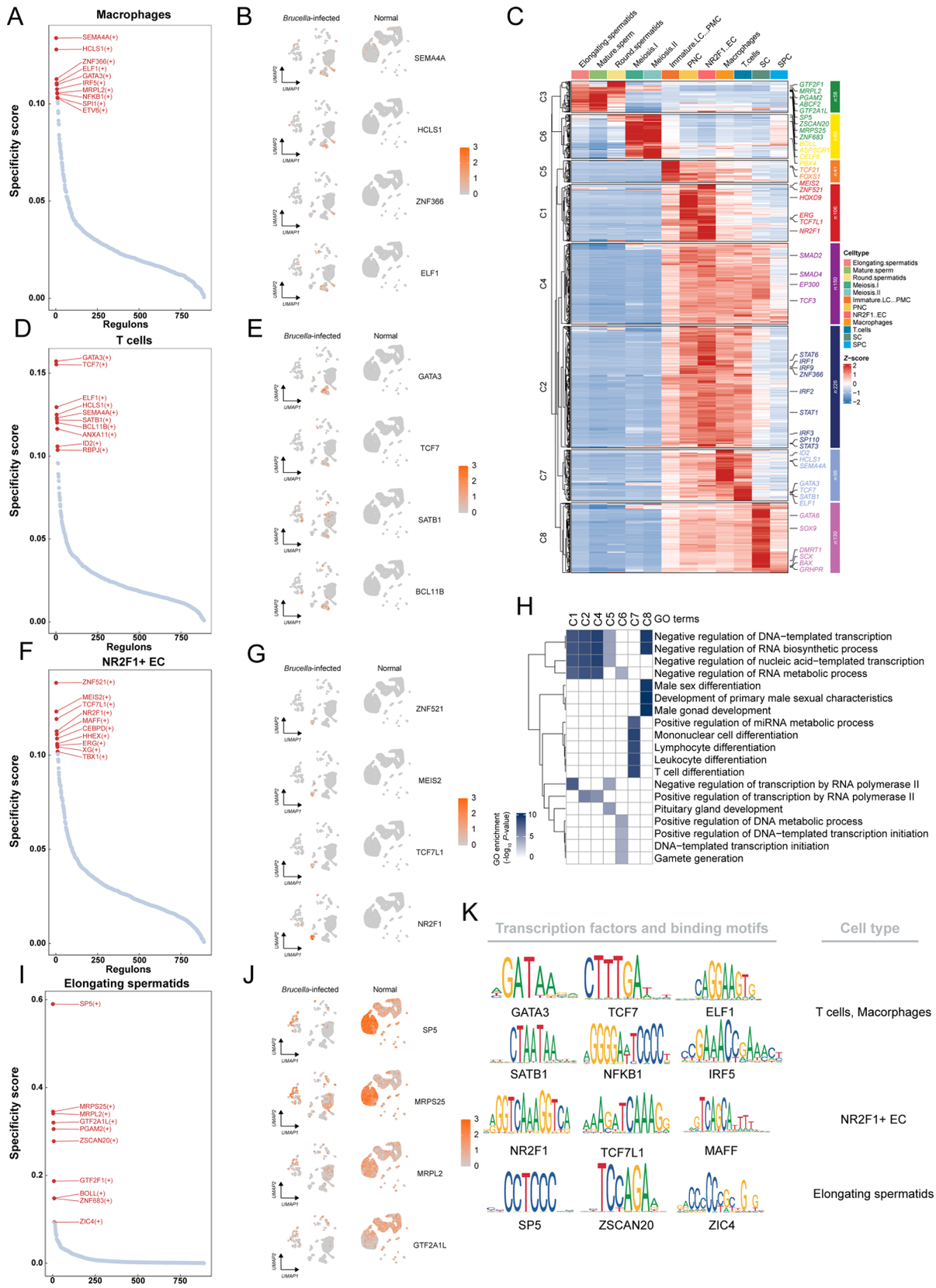

Figure 6 SCENIC-based inference of transcriptional regulatory networks in testicular cell types

A, B: Macrophages. A: Ranking of macrophage regulons based on regulon specificity score (RSS). B: UMAP plots highlighting top four macrophage regulons across different samples. C: Heatmap of regulon clusters derived from RSS matrix, annotated with representative transcription factors and associated cell types. D, E: Same analyses as in A, B, but for T cells. F, G: Same analyses as in A, B, but for NR2F1^{+} endothelial cells (ECs). H: Heatmap showing significance (*P*-value) of GO term enrichment for genes in each regulon in panel C I, J: Same analyses as in A, B, but for elongating spermatids. K: Overview of regulon activity patterns across different testicular cell types.

transcriptional states among T cells in *Brucella*-infected testes. State 1 was characterized by enrichment of biosynthetic and metabolic pathways, consistent with the observation of increased mitochondrial metabolism and intracellular transcriptional activity during adaptive immune responses (Hunt et al., 2024; Lopes et al., 2021; Xu et al., 2021). In contrast, States 2 and 3 exhibited transcriptional signatures indicative of immunological activation, including robust up-regulation of *LOC108633460* and *LOC102172138*, which encode components of BOLA class I molecules—implicating enhanced MHC I-mediated intracellular antigen presentation (Colbert et al., 2022). This is particularly relevant given that *Brucella*, as an intracellular pathogen, exploits Sec61 to localize to the endoplasmic reticulum and facilitate antigen translocation across endosomal membranes (Zehner et al., 2015). These findings suggest that activation of cytotoxic T cells is essential for the clearance of intracellular *Brucella* and point to intracellular antigen presentation as a mechanistic axis of host defense.

Additionally, States 2 and 3 showed elevated expression of *IGTB2*, aligning with cellular communication analyses (Figures 2D, 4E) and implicating ICAM signaling in T cell activation and migration. Several molecules, such as *SEMA4A*, *CCL5*, and *LCP2*, were also associated with sustained activation phenotypes (Figure 2D). WGCNA identified key immune network components potentially involved in anti-*Brucella* responses, including *TXNIP*, *LOC102181202* (MHC I family), *B2M*, *KCTD12*, *VIM*, and *TBL1XR1*. To further define regulatory hierarchies, an immune cell transcriptional network was constructed, revealing shared regulators between T cells and macrophages, notably *SEMA4A*, *HCLS1*, *ELF1*, and *GATA3*. SEMA4A has been shown to initiate early T cell activation (Kumanogoh et al., 2002; Naito et al., 2023) and regulate proinflammatory cytokines such as IL-1β, TNFα, and IL6, reinforcing inflammatory signaling (Wang et al., 2015; Zhang et al., 2019). GATA3, a known determinant of T cell proliferation and maintenance (De Obaldia & Bhandoola, 2015; Kasal et al., 2021; Trujillo-Ochoa et al., 2023), also emerged as a significant regulator in the infected testes, although its context-specific role requires further investigation. In addition, the T cell network highlighted lineage-specific regulators, including *TCF7*, *SATB1*, *BCL11B*, *ID2*, and *RBPJ*. Notably, *TCF7* exhibited a high RSS, consistent with its established role in T and innate lymphoid cell lineage commitment (De Obaldia & Bhandoola, 2015; Pais Ferreira et al., 2020; Raghu et al., 2019) and its capacity to maintain stem-like properties in $CD4^+$ and $CD8^+$ T cells under chronic stimulation (Raghu et al., 2019), potentially contributing to sustained effector responses during persistent *Brucella* infection. Future studies should explore the functional contributions of these regulatory factors to effective host defense.

Brucella infection significantly altered intercellular signaling networks in the testis, potentially contributing to spermatogenic failure. The number of predicted ligand-receptor interactions was markedly increased in infected samples compared to normal samples, indicating widespread disruption of cell-cell communication. However, key signaling pathways essential for maintaining testicular integrity were down-regulated. In particular, CD39 and JAM signaling—both critical for preserving the blood-testis barrier—were markedly down-regulated in *Brucella*-infected samples. CD39 has been implicated in maintaining immune privilege within the testis (Jenabian et al., 2016; Takenaka et al., 2016), while JAM family proteins support the structural integrity of tight junctions at the blood-testis barrier (Yan & Cheng, 2005; Yan et al., 2008). Their down-regulation suggests that *Brucella* infection disrupts signaling pathways critical for sustaining the blood-testis barrier, thereby impairing spermatogenesis. Conversely, proinflammatory signaling pathways such as CD45 and MIF were up-regulated in the infected samples, reflecting heightened immune responses (Jung et al., 2021; Sumaiya et al., 2022). *IL6ST*, a receptor for multiple cytokines involved in immunoregulation, was significantly up-regulated in *Brucella*-infected testes, further indicating disruption of immune activity during infection. Interestingly, a distinct endothelial cell population characterized by high *NR2F1* expression was enriched in *Brucella*-infected tissue. This subset showed transcriptional signatures of TGFβ and WNT pathway activation and demonstrated extensive ligand-receptor interactions with other cell types, including the ADGRE5-CD55 pathway, which is associated with immune cell recruitment and migration (Liu et al., 2022, 2024a). Future studies should investigate the mechanisms by which $NR2F1^+$ endothelial cells recruit immune cells during *Brucella* infection.

In summary, single-cell transcriptomic profiling of the *Brucella*-infected goat testis revealed extensive remodeling of both germ and somatic populations, providing a detailed molecular framework for understanding testicular responses to brucellosis. Distinct transcriptional signatures were observed in immune cells, highlighting key signaling pathways associated with host defense.

DATA AVAILABILITY

All software tools can be found online (see Supplementary Table S1). The single-cell sequencing data generated in this study have been deposited in the NCBI database (BioProjectID PRJNA1353656), Genome Sequence Archive (https://ngdc.cncb.ac.cn/gsa) (GSA: CRA023324), and Science Data Bank (DOI: 10.57760/sciencedb.j00139.00307). Any additional information required to reanalyze the data reported in this paper is available from the lead contact upon request.

SUPPLEMENTARY DATA

Supplementary data to this article can be found online.

COMPETING INTERESTS

The authors declare that they have no competing interests.

AUTHORS' CONTRIBUTIONS

J.L.H., H.S.Y., H.J.Z., and N.L. conceived and supervised the project and designed the experiments. W.B.C. conducted computational analysis and validation experiments. C.L.W., S.C.W., M.F.Z., and B.H. characterized the goats. X.L., D.H.Y., and W.P.W. performed staining experiments. The manuscript was written by W.B.C., H.S.Y., and J.L.H. with input and agreement of all authors. All authors read and approved the final version of the manuscript.

ACKNOWLEDGMENTS

We thank the high-performance computing platform of Northwest A&F University (NWAFU) for providing computing resources.

REFERENCES

Alfano M, Tascini AS, Pederzoli F, et al. 2021. Aging, inflammation and DNA damage in the somatic testicular niche with idiopathic germ cell aplasia. *Nature Communications*, **12**(1): 5205.

Athanasouli P, Balli M, De Jaime-Soguero A, et al. 2023. The Wnt/TCF7L1 transcriptional repressor axis drives primitive endoderm formation by

antagonizing naive and formative pluripotency. *Nature Communications*, **14**(1): 1210.

Audas TE, Li Y, Liang GQ, et al. 2008. A novel protein, Luman/CREB3 recruitment factor, inhibits Luman activation of the unfolded protein response. *Molecular and Cellular Biology*, **28**(12): 3952–3966.

Byndloss MX, Tsolis RM. 2016. *Brucella* spp. virulence factors and immunity. *Annual Review of Animal Biosciences*, **4**: 111–127.

Celli J. 2019. The intracellular life cycle of *Brucella* spp. *Microbiology Spectrum*, **7**(2), doi: 10.1128/microbiolspec.BAI-0006-2019.

Celli J, de Chastellier C, Franchini DM, et al. 2003. *Brucella* evades macrophage killing via VirB-dependent sustained interactions with the endoplasmic reticulum. *The Journal of Experimental Medicine*, **198**(4): 545–556.

Chen ELY, Thompson PK, Zúñiga-Pflücker JC. 2019. RBPJ-dependent Notch signaling initiates the T cell program in a subset of thymus-seeding progenitors. *Nature Immunology*, **20**(11): 1456–1468.

Chen WB, Zhang MF, Yang F, et al. 2024a. Applications of single-cell RNA sequencing in spermatogenesis and molecular evolution. *Zoological Research*, **45**(3): 575–585.

Chen ZY, Inague A, Kaushal K, et al. 2024b. PRDX6 contributes to selenocysteine metabolism and ferroptosis resistance. *Molecular Cell*, **84**(23): 4645–4659. e9.

Cheong A, Archambault D, Degani R, et al. 2020. Nuclear-encoded mitochondrial ribosomal proteins are required to initiate gastrulation. *Development*, **147**(10): dev188714.

Colbert JD, Cruz FM, Baer CE, et al. 2022. Tetraspanin-5-mediated MHC class I clustering is required for optimal CD8 T cell activation. *Proceedings of the National Academy of Sciences of the United States of America*, **119**(42): e2122188119.

Danileviciute E, Zeng N, Capelle CM, et al. 2022. PARK7/DJ-1 promotes pyruvate dehydrogenase activity and maintains T_{reg} homeostasis during ageing. *Nature Metabolism*, **4**(5): 589–607.

De Bolle X, Crosson S, Matroule JY, et al. 2015. *Brucella abortus* cell cycle and infection are coordinated. *Trends in Microbiology*, **23**(12): 812–821.

De Obaldia ME, Bhandoola A. 2015. Transcriptional regulation of innate and adaptive lymphocyte lineages. *Annual Review of Immunology*, **33**: 607–642.

Di Persio S, Tekath T, Siebert-Kuss LM, et al. 2021. Single-cell RNA-seq unravels alterations of the human spermatogonial stem cell compartment in patients with impaired spermatogenesis. *Cell Reports Medicine*, **2**(9): 100395.

Dorneles EMS, Sriranganathan N, Lage AP. 2015. Recent advances in *Brucella abortus* vaccines. *Veterinary Research*, **46**(1): 76.

Eto M. 2009. Regulation of cellular protein phosphatase-1 (PP1) by phosphorylation of the CPI-17 family, C-kinase-activated PP1 inhibitors. *Journal of Biological Chemistry*, **284**(51): 35273–35277.

Fugier E, Pappas G, Gorvel JP. 2007. Virulence factors in brucellosis: implications for aetiopathogenesis and treatment. *Expert Reviews in Molecular Medicine*, **9**(35): 1–10.

Galber C, Minervini G, Cannino G, et al. 2021. The f subunit of human ATP synthase is essential for normal mitochondrial morphology and permeability transition. *Cell Reports*, **35**(6): 109111.

Guo JT, Sosa E, Chitiashvili T, et al. 2021. Single-cell analysis of the developing human testis reveals somatic niche cell specification and fetal germline stem cell establishment. *Cell Stem Cell*, **28**(4): 764–778. e4.

Hao YH, Stuart T, Kowalski MH, et al. 2024. Dictionary learning for integrative, multimodal and scalable single-cell analysis. *Nature Biotechnology*, **42**(2): 293–304.

Hashwah H, Schmid CA, Kasser S, et al. 2017. Inactivation of CREBBP expands the germinal center B cell compartment, down-regulates MHCII expression and promotes DLBCL growth. *Proceedings of the National Academy of Sciences of the United States of America*, **114**(36): 9701–9706.

Hassaneen ASA, Anis A, Nour SY, et al. 2024. Poor semen quality is associated with impaired antioxidant response and acute phase proteins and is likely mediated by high cortisol levels in *Brucella*-seropositive dromedary camel bulls. *Scientific Reports*, **14**(1): 27816.

Hu H, Tian MX, Li P, et al. 2020. *Brucella* infection regulates thioredoxin-interacting protein expression to facilitate intracellular survival by reducing the production of nitric oxide and reactive oxygen species. *The Journal of Immunology*, **204**(3): 632–643.

Huggins IJ, Bos T, Gaylord O, et al. 2017. The WNT target SP5 negatively regulates WNT transcriptional programs in human pluripotent stem cells. *Nature Communications*, **8**(1): 1034.

Hunt EG, Hurst KE, Riesenberg BP, et al. 2024. Acetyl-CoA carboxylase obstructs $CD8^+$ T cell lipid utilization in the tumor microenvironment. *Cell Metabolism*, **36**(5): 969–983. e10.

Jenabian MA, Costiniuk CT, Mehraj V, et al. 2016. Immune tolerance properties of the testicular tissue as a viral sanctuary site in ART-treated HIV-infected adults. *AIDS*, **30**(18): 2777–2786.

Ji HB, Gupta A, Okamoto S, et al. 2002. T cell-specific expression of the murine *CD3δ* promoter. *Journal of Biological Chemistry*, **277**(49): 47898–47906.

Jin SQ, Guerrero-Juarez CF, Zhang LH, et al. 2021. Inference and analysis of cell-cell communication using CellChat. *Nature Communications*, **12**(1): 1088.

Jung Y, Wen L, Altman A, et al. 2021. CD45 pre-exclusion from the tips of T cell microvilli prior to antigen recognition. *Nature Communications*, **12**(1): 3872.

Kasal DN, Liang ZT, Hollinger MK, et al. 2021. A *Gata3* enhancer necessary for ILC2 development and function. *Proceedings of the National Academy of Sciences of the United States of America*, **118**(32): e2106311118.

Korsunsky I, Millard N, Fan J, et al. 2019. Fast, sensitive and accurate integration of single-cell data with Harmony. *Nature Methods*, **16**(12): 1289–1296.

Kulalert W, Wells AC, Link VM, et al. 2024. The neuroimmune CGRP-RAMP1 axis tunes cutaneous adaptive immunity to the microbiota. *Proceedings of the National Academy of Sciences of the United States of America*, **121**(11): e2322574121.

Kumanogoh A, Marukawa S, Suzuki K, et al. 2002. Class IV semaphorin Sema4A enhances T-cell activation and interacts with Tim-2. *Nature*, **419**(6907): 629–633.

Lamers C, Mastellos DC, Ricklin D, et al. 2022. Compstatins: the dawn of clinical C3-targeted complement inhibition. *Trends in Pharmacological Sciences*, **43**(8): 629–640.

Langfelder P, Horvath S. 2008. WGCNA: an R package for weighted correlation network analysis. *BMC Bioinformatics*, **9**: 559.

Lawrence T, Natoli G. 2011. Transcriptional regulation of macrophage polarization: enabling diversity with identity. *Nature Reviews Immunology*, **11**(11): 750–761.

Liu D, Duan LH, Rodda LB, et al. 2022. CD97 promotes spleen dendritic cell homeostasis through the mechanosensing of red blood cells. *Science*, **375**(6581): eabi5965.

Liu D, Winer BY, Chou MY, et al. 2024a. Dynamic encounters with red blood cells trigger splenic marginal zone B cell retention and function. *Nature Immunology*, **25**(1): 142–154.

Liu Q, Zhang J, Guo CC, et al. 2024b. Proteogenomic characterization of small cell lung cancer identifies biological insights and subtype-specific therapeutic strategies. *Cell*, **187**(1): 184–203. e28.

Liu ZG, Gao LP, Wang M, et al. 2024c. Long ignored but making a comeback: a worldwide epidemiological evolution of human brucellosis. *Emerging Microbes & Infections*, **13**(1): 2290839.

Lopes N, Mcintyre C, Martin S, et al. 2021. Distinct metabolic programs established in the thymus control effector functions of γδ T cell subsets in tumor microenvironments. *Nature Immunology*, **22**(2): 179–192.

Ma XD, Xu SD, Hao SH, et al. 2022. KLF16 enhances stress tolerance of colorectal carcinomas by modulating nucleolar homeostasis and translational reprogramming. *Molecular Therapy*, **30**(8): 2828–2843.

Miraglia MC, Scian R, Samartino CG, et al. 2013. *Brucella abortus* induces TNF-α-dependent astroglial MMP-9 secretion through mitogen-activated protein kinases. *Journal of Neuroinflammation*, **10**: 819.

Naito Y, Koyama S, Masuhiro K, et al. 2023. Tumor-derived semaphorin 4A

improves PD-1-blocking antibody efficacy by enhancing CD8$^+$ T cell cytotoxicity and proliferation. *Science Advances*, **9**(20): eade0718.
Nguyen H, Rendl M, Fuchs E. 2006. Tcf3 governs stem cell features and represses cell fate determination in skin. *Cell*, **127**(1): 171–183.
Oatley JM, Brinster RL. 2012. The germline stem cell niche unit in mammalian testes. *Physiological Reviews*, **92**(2): 577–595.
Osman EEA, Neamati N. 2024. Ironing out the mechanism of gp130 signaling. *Pharmacological Reviews*, **76**(6): 1399–1443.
Otasek D, Morris JH, Bouças J, et al. 2019. Cytoscape Automation: empowering workflow-based network analysis. *Genome Biology*, **20**(1): 185.
Pais Ferreira D, Silva JG, Wyss T, et al. 2020. Central memory CD8$^+$ T cells derive from stem-like *Tcf7*^{hi} effector cells in the absence of cytotoxic differentiation. *Immunity*, **53**(5): 985–1000. e11.
Pappas G, Akritidis N, Bosilkovski M, et al. 2005. Brucellosis. *The New England Journal of Medicine*, **352**(22): 2325–2336.
Qiu XJ, Hill A, Packer J, et al. 2017. Single-cell mRNA quantification and differential analysis with Census. *Nature Methods*, **14**(3): 309–315.
Qureshi KA, Parvez A, Fahmy NA, et al. 2023. Brucellosis: epidemiology, pathogenesis, diagnosis and treatment-a comprehensive review. *Annals of Medicine*, **55**(2): 2295398.
Rabbani M, Zheng XN, Manske GL, et al. 2022. Decoding the spermatogenesis program: new insights from transcriptomic analyses. *Annual Review of Genetics*, **56**: 339–368.
Raghu D, Xue HH, Mielke LA. 2019. Control of lymphocyte fate, infection, and tumor immunity by TCF-1. *Trends in Immunology*, **40**(12): 1149–1162.
Sandberg ML, Sutton SE, Pletcher MT, et al. 2005. c-Myb and p300 regulate hematopoietic stem cell proliferation and differentiation. *Developmental Cell*, **8**(2): 153–166.
Savasci U, Zor M, Karakas A, et al. 2014. Brucellar epididymo-orchitis: a retrospective multicenter study of 28 cases and review of the literature. *Travel Medicine and Infectious Disease*, **12**(6): 667–672.
Schönenberger MJ, Krek W, Kovacs WJ. 2015. EPAS1/HIF-2α is a driver of mammalian pexophagy. *Autophagy*, **11**(6): 967–969.
Sedzicki J, Tschon T, Low SH, et al. 2018. 3D correlative electron microscopy reveals continuity of *Brucella*-containing vacuoles with the endoplasmic reticulum. *Journal of Cell Science*, **131**(4): jcs210799.
Shibata T, Makino A, Ogata R, et al. 2020. Respiratory syncytial virus infection exacerbates pneumococcal pneumonia via Gas6/Axl-mediated macrophage polarization. *The Journal of Clinical Investigation*, **130**(6): 3021–3037.
Shin JW, Suzuki T, Ninomiya N, et al. 2012. Establishment of single-cell screening system for the rapid identification of transcriptional modulators involved in direct cell reprogramming. *Nucleic Acids Research*, **40**(21): e165.
Sohni A, Tan K, Song HW, et al. 2019. The neonatal and adult human testis defined at the single-cell level. *Cell Reports*, **26**(6): 1501–1517. e4.
Stuart T, Butler A, Hoffman P, et al. 2019. Comprehensive integration of single-cell data. *Cell*, **177**(7): 1888–1902. e21.
Sumaiya K, Langford D, Natarajaseenivasan K, et al. 2022. Macrophage migration inhibitory factor (MIF): a multifaceted cytokine regulated by genetic and physiological strategies. *Pharmacology & Therapeutics*, **233**: 108024.
Sung AY, Guerra RM, Steenberge LH, et al. 2024. Systematic analysis of NDUFAF6 in complex I assembly and mitochondrial disease. *Nature Metabolism*, **6**(6): 1128–1142.
Takenaka MC, Robson S, Quintana FJ. 2016. Regulation of the T cell response by CD39. *Trends in Immunology*, **37**(7): 427–439.
Trujillo-Ochoa JL, Kazemian M, Afzali B. 2023. The role of transcription factors in shaping regulatory T cell identity. *Nature Reviews Immunology*, **23**(12): 842–856.
Van de Sande B, Flerin C, Davie K, et al. 2020. A scalable SCENIC workflow for single-cell gene regulatory network analysis. *Nature Protocols*, **15**(7): 2247–2276.
Villar J, Cros A, De Juan A, et al. 2023a. ETV3 and ETV6 enable monocyte differentiation into dendritic cells by repressing macrophage fate commitment. *Nature Immunology*, **24**(1): 84–95.
Villar J, Ouaknin L, Cros A, et al. 2023b. Monocytes differentiate along two alternative pathways during sterile inflammation. *EMBO Reports*, **24**(7): e56308.
Wan YY. 2014. GATA3: a master of many trades in immune regulation. *Trends in Immunology*, **35**(6): 233–242.
Wang CQF, Cheng CY. 2007. A seamless trespass: germ cell migration across the seminiferous epithelium during spermatogenesis. *The Journal of Cell Biology*, **178**(4): 549–556.
Wang L, Song GH, Zheng YB, et al. 2015. Expression of Semaphorin 4A and its potential role in rheumatoid arthritis. *Arthritis Research & Therapy*, **17**(1): 227.
Wang M, Kaufman RJ. 2016. Protein misfolding in the endoplasmic reticulum as a conduit to human disease. *Nature*, **529**(7586): 326–335.
Wells KM, He K, Pandey A, et al. 2022. *Brucella* activates the host RIDD pathway to subvert BLOS1-directed immune defense. *eLife*, **11**: e73625.
Wu GL, Ma ZQ, Cheng YC, et al. 2018. Targeting Gas6/TAM in cancer cells and tumor microenvironment. *Molecular Cancer*, **17**(1): 20.
Xu K, Yin N, Peng M, et al. 2021. Glycolytic ATP fuels phosphoinositide 3-kinase signaling to support effector T helper 17 cell responses. *Immunity*, **54**(5): 976–987. e7.
Yan HHN, Cheng CY. 2005. Blood-testis barrier dynamics are regulated by an engagement/disengagement mechanism between tight and adherens junctions via peripheral adaptors. *Proceedings of the National Academy of Sciences of the United States of America*, **102**(33): 11722–11727.
Yan HHN, Mruk DD, Lee WM, et al. 2008. Blood-testis barrier dynamics are regulated by testosterone and cytokines *via* their differential effects on the kinetics of protein endocytosis and recycling in Sertoli cells. *The FASEB Journal*, **22**(6): 1945–1959.
Yang QH, Fujii W, Kaji N, et al. 2018. The essential role of phospho-T38 CPI-17 in the maintenance of physiological blood pressure using genetically modified mice. *The FASEB Journal*, **32**(4): 2095–2109.
Yin SL, Tao YJ, Li TL, et al. 2024. Itaconate facilitates viral infection via alkylating GDI2 and retaining Rab GTPase on the membrane. *Signal Transduction and Targeted Therapy*, **9**(1): 371.
Yu JW, Li S, Wang L, et al. 2022. Pathogenesis of *Brucella* epididymoorchitis-game of *Brucella* death. *Critical Reviews in Microbiology*, **48**(1): 96–120.
Yu XW, Li TT, Du XM, et al. 2021. Single-cell RNA sequencing reveals atlas of dairy goat testis cells. *Zoological Research*, **42**(4): 401–405.
Zehner M, Marschall AL, Bos E, et al. 2015. The translocon protein Sec61 mediates antigen transport from endosomes in the cytosol for cross-presentation to CD8$^+$ T cells. *Immunity*, **42**(5): 850–863.
Zhan YQ, Xu DW, Tian YZ, et al. 2022. Novel role of macrophage TXNIP-mediated CYLD-NRF2-OASL1 axis in stress-induced liver inflammation and cell death. *JHEP Reports*, **4**(9): 100532.
Zhang GQ, Lu JN, Zheng JW, et al. 2024. Spi1 regulates the microglial/macrophage inflammatory response via the PI3K/AKT/mTOR signaling pathway after intracerebral hemorrhage. *Neural Regeneration Research*, **19**(1): 161–170.
Zhang H, Wei QS, Xiang XB, et al. 2019. Semaphorin 4A acts in a feed-forward loop with NF-κB pathway to exacerbate catabolic effect of IL-1β on chondrocytes. *International Immunopharmacology*, **69**: 88–94.
Zhao ST, Zhu WW, Xue SP, et al. 2014. Testicular defense systems: immune privilege and innate immunity. *Cellular & Molecular Immunology*, **11**(5): 428–437.
Zou QX, Yang LL, Shi RN, et al. 2021. Proteostasis regulated by testis-specific ribosomal protein RPL39L maintains mouse spermatogenesis. *iScience*, **24**(12): 103396.